# $\gamma\gamma + E_{\mathrm{T}}^{\mathrm{miss}}$ Study

Shikma Bressler[*1], Stefania Gori[†2], Rafael Teixeira de Lima[‡3], Abdollah Mohammadi[§4], Toyoko Orimoto[¶3] and Jessie Shelton[‖5]

[1]Weizmann Institute of Science, Israel
[2]Perimeter Institute for theoretical physics, Canada and Cincinnati University, USA
[3]Northeastern University, USA
[4]Kansas State University, USA
[5]University of Illinois at Urbana-Champaign, USA

## 1 Introduction

Exotic decays of the Higgs boson can produce the final state consisting of two photons and missing transverse energy ($E_{\mathrm{T}}^{\mathrm{miss}}$) [?]. In the non-resonant case, the photons arise from opposite sides of the initial two-body decay: $h \rightarrow XX, X \rightarrow \gamma Y$, where $Y$ is a stable neutral particle. For instance, such a decay can occur within general gauge mediation models of supersymmetry, in which the $X$ corresponds to a neutralino NLSP with mass less than half the Higgs mass, and the $Y$ corresponds to a gravitino LSP [?, ?, ?]. In the resonant case, the photons are produced through an intermediate resonance: $h \rightarrow S_1 S_2$, with $S_1 \rightarrow \gamma\gamma$ on one side of the decay, while $S_2$ escapes detection, appearing as $E_{\mathrm{T}}^{\mathrm{miss}}$ in the detector. The resonant signal benefits from a peak in the diphoton invariant mass spectrum. The Feynman diagrams for the non-resonant and resonant decays can be seen in Figure ??.

Previous searches for the $\gamma\gamma + E_{\mathrm{T}}^{\mathrm{miss}}$ final state in the low energy regime include searches for the non-resonant decay in the supersymmetric scenario described above. CMS and ATLAS have set upper limits on the branching ratio of this decay, with the Higgs boson produced in association with a $Z$ boson [?] and through vector boson fusion [?].

In this study, we devise a search strategy for the $\gamma\gamma + E_{\mathrm{T}}^{\mathrm{miss}}$ final state, motivated by the exotic decays of the Higgs described above. We estimate the sensitivity of this search for 100 fb$^{-1}$ of $\sqrt{s} = 14$ TeV $pp$ data from the LHC.

## 2 Methodology

### 2.1 Simulation Samples

Signal and background Monte Carlo (MC) samples were generated with Madgraph 5 [?] and hadronized with PYTHIA 8 [?], with the detector simulation provided by DELPHES 3 [?]. The samples were produced at $\sqrt{s} = 14$ TeV.

---

[*]Shikma.Bressler@cern.ch

[†]sgori@perimeterinstitute.ca

[‡]rafael.teixeira.de.lima@cern.ch

[§]Abdollah.Mohammadi@cern.ch

[¶]Toyoko.Orimoto@cern.ch
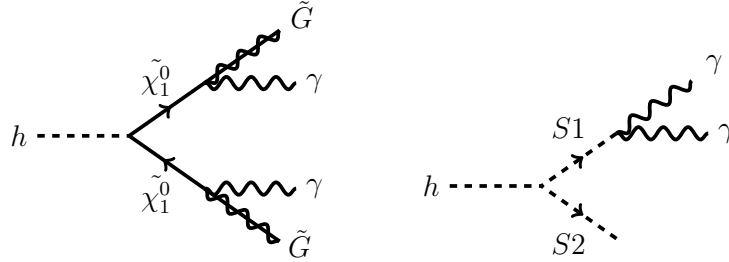
[‖]jshelton137@gmail.com

Figure 1: Feynman diagrams for the (left) the non-resonant and (right) resonant signal scenarios.

The object reconstruction and identification are performed with DELPHES, according to the information provided in the detector configuration card. For the photons reconstruction and identification, we assume an efficiency of 95% in the electromagnetic calorimeter barrel ($|\eta| < 1.5$) and 85% in the endcap ($1.5 < |\eta| < 2.5$). We also impose an isolation cut on the photons by requiring all particle flow candidates within a cone of $\Delta R < 0.3$ to have an energy ratio less than 0.1 with respect to the photon candidate. For muons, we assume an efficiency of 95% for the whole detector acceptance ($|\eta| < 2.5$). An isolation cut similar to the photons is also applied. Jets are reconstructed with the anti-$k_T$ algorithm with $R = 0.4$.

### 2.1.1 Signal MC Samples

The signal for the non-resonant case was based on the supersymmetric cascade decay of the Higgs boson into two neutralinos, which subsequently decay into two gravitinos and two photons (Figure **??**, left). This class of models has been implemented in FeynRules [**?**] and generated via Madgraph 5. We assume a gravitino mass close to zero, which is consistent with gauge mediated low-scale SUSY breaking models with $\sqrt{f} \approx$ TeV [**?**]. We simulate neutralino masses in the range $[10, 60]$ GeV in steps of 5 GeV, with 100,000 events per mass point.

For the resonant case, we assume the Higgs boson decays into two scalar particles, $S_1$ and $S_2$ (Figure **??**, right). One of the scalars then decays into two photons, while the other escapes detection. For this study, we assume the masses of these two particles are the same; this choice was made for simplicity, but for detailed studies, more combinations should be investigated. We generate samples with $M_1 = M_2 = [10, 60]$ GeV, in steps of 5 GeV, with 100,000 events per mass point.

We investigate the production of the Higgs boson through both gluon fusion and associated production with a $Z$ boson ($ZH$), with the $Z$ boson decaying to two muons. The inclusion of the dielectron decay of the $Z$ can also be considered for future studies. A branching ratio of $B(H \rightarrow \gamma\gamma + E_T^{miss}) = 10\%$ is assumed for the signal. This value of the branching ratio was chosen to be within the current bounds on the Higgs boson width, yet close to the 8 TeV limits from the search for Higgs decays to the monophoton final state ($H \rightarrow \gamma + E_T^{miss}$) [**?**].

### 2.1.2 Background MC Samples

Although this analysis is not guaranteed to be entirely free from QCD multi-jet backgrounds, it has been shown in similar analyses (such as [**?**]) that it is possible to reduce the QCD to a sub-dominant contribution. As such, the remaining backgrounds for this analysis arise predominantly from the single boson ($\gamma/Z/W$) plus jets and diboson processes.

The background samples were modeled using the Snowmass LHE simulation samples [**?**]. They consist of single boson samples ($\gamma/Z/W$) with at least one jet and inclusive diboson ($\gamma\gamma/Z\gamma/W\gamma/WW/ZZ/WZ$) samples. The samples include both hadronic and leptonic decays of the $W$ and $Z$ bosons. The cross sections used for normalizing the single boson samples were estimated with MCFM [**?**], assuming an efficiency of 15% for the 1 jet requirement (obtained with Madgraph). For the diboson samples, the cross sections used were estimated from the reference [**?**]. The cross sections and number of events in the samples are shown in Table **??**.

## 2.2 Event Selection

### 2.2.1 Trigger Projections

For the $ZH$ channel, the trigger strategy is expected to be straightforward and can be based on the decay of the $Z$ to two muons. On the other hand, triggering is one of the main challenges for the gluon fusion channel, since the final state consists of two soft photons plus missing energy. The standard triggers used for $H \to \gamma\gamma$ analyses typically have a diphoton invariant mass cut which makes it incompatible with the low energy spectrum of this analysis. However, we have identified three possible trigger strategies for this channel, based on unprescaled triggers used by the CMS experiment in Run-2:

- Asymmetric Diphoton Trigger: This trigger requires two photons with different $E_T$ and trigger-level identification requirements, plus a diphoton invariant mass cut. This type of trigger usually has a non-negligible turn-on curve in the leading and subleading photon $E_T$.

- Symmetric Diphoton Trigger: This trigger requires two photons with the same $E_T$ requirement, without any extra requirement.

- $\gamma + E_{\mathrm{T}}^{\mathrm{miss}}$ Trigger: This trigger requires only one barrel photon passing identification requirements and a $E_T$ requirement that is usually higher than the previous two triggers. In addition, there is a calorimetric $E_{\mathrm{T}}^{\mathrm{miss}}$ requirement. We expect non-negligible turn-on curves with respect to both photon and $E_{\mathrm{T}}^{\mathrm{miss}}$ for this trigger.

The three triggers described here represent different selection strategies that were investigated and will be described below.

### 2.2.2 Offline Selection

The gluon fusion selection is based on the diphoton selection and must reflect the chosen trigger strategy, while maintaining a good signal efficiency. The $ZH$-produced signal events are tagged through the decay of the $Z$ boson to muons, minimizing the largest backgrounds. The photon selection is chosen to maximize the signal acceptance in the $ZH$ case, with $E_T$ thresholds as low as possible. The final event selection requirements for the gluon fusion and $ZH$ channels are summarized in Table **??**. On this table, we use the following definitions for transverse mass:

$$M_T(\gamma\gamma, E_{\mathrm{T}}^{\mathrm{miss}}) = \sqrt{2E_T(\gamma\gamma)E_{\mathrm{T}}^{\mathrm{miss}}(1 - \cos(\Delta\phi(\gamma\gamma, E_{\mathrm{T}}^{\mathrm{miss}}))}, \tag{1}$$

$$M_T(\gamma\gamma + E_{\mathrm{T}}^{\mathrm{miss}}, \mu\mu) = \sqrt{2E_T(\gamma\gamma + E_{\mathrm{T}}^{\mathrm{miss}})p_T(\mu\mu)(1 - \cos(\Delta\phi(\gamma\gamma + E_{\mathrm{T}}^{\mathrm{miss}}, \mu\mu))}. \tag{2}$$

To exploit the topology of the resonant signature, we apply an additional requirement of a 20 GeV mass window, in the diphoton invariant mass distribution ($M(\gamma\gamma)$), around the signal mass

3

| | gluon Fusion | | | $ZH$ |
| --- | --- | --- | --- | --- |
| Variable | Asymmetric $\gamma\gamma$ | Symmetric $\gamma\gamma$ | $\gamma + E_{\mathrm{T}}^{\mathrm{miss}}$ | |
| Number of photons | $> 1$ | $> 1$ | $> 1$ | $> 1$ |
| $p_T(\gamma_1)$ | $> 45$ GeV | $> 40$ GeV | $> 55$ GeV | $> 20$ GeV |
| $|\eta(\gamma_1)|$ | $< 2.5$ | $< 2.5$ | $< 1.4$ | $< 2.5$ |
| $p_T(\gamma_2)$ | $> 30$ GeV | $> 40$ GeV | $> 20$ GeV | $> 20$ GeV |
| $|\eta(\gamma_2)|$ | $< 2.5$ | $< 2.5$ | $< 2.5$ | $< 2.5$ |
| $M(\gamma\gamma)$ | $\in [15, 100]$ GeV | $< 100$ GeV | $< 100$ GeV | $< 100$ GeV |
| $E_{\mathrm{T}}^{\mathrm{miss}}$ | $> 90$ GeV | $> 90$ GeV | $> 90$ GeV | $> 60$ GeV |
| $M_T(\gamma\gamma, E_{\mathrm{T}}^{\mathrm{miss}})$ | $< 140$ GeV | $< 140$ GeV | $< 140$ GeV | $< 140$ GeV |
| $\Delta\phi(\gamma\gamma, E_{\mathrm{T}}^{\mathrm{miss}})$ | $< 1.5$ | $< 1.5$ | $< 1.5$ | $< 1.5$ |
| Number of leptons | $< 1$ | $< 1$ | $< 1$ | 2 muons |
| $p_T(\mu_{1,2})$ | - | - | - | $> 20$ GeV |
| $|\eta(\mu_{1,2})|$ | - | - | - | $< 2.5$ |
| $M(\mu\mu)$ | - | - | - | $\in [75, 115]$ GeV |
| $M_T(\gamma\gamma + E_{\mathrm{T}}^{\mathrm{miss}}, \mu\mu)$ | - | - | - | $> 400$ GeV |

Table 1: Analysis selection for the gluon fusion channel (for each trigger scenario) and the $ZH$ channel.

($M_1$). The efficiencies for each individual process and the different searches, after the full selection (without the $M(\gamma\gamma)$ mass window requirement), are shown in Table **??**.

## 2.3 Background Estimation for Misidentified Photons

Background processes with mis-identified (or "fake") photons, such as jets and electrons misidentified as photons, that pass the final selection generally have very low efficiency at the LHC. Nonetheless, such backgrounds may be non-negligible since the production cross-sections can be large. Such mis-identification rates are typically measured with data-driven methods at the LHC. Although this study was limited by MC statistics in measuring fake photon backgrounds, a method was developed to mitigate this problem, which we describe below.

The object reconstruction and selection is done at DELPHES level, where, given the photon identification requirements described in Section **??**, we obtain an associated fake rate. These fake rates are accounted for in the overall efficiencies in Table **??**. In order to bypass the efficiency loss due to the small fake rates, we select jets and electrons as fake photon candidates. For the background processes with one prompt photon ($\gamma$+jets, $W\gamma$ and $Z\gamma$), we select one fake photon candidate. For the processes with no prompt photons ($W/Z$+jets, $WW$, $WZ$ and $ZZ$), we select two fake photon candidates. No fake photon selection is done for the $\gamma\gamma$+jets sample.

With the assumption of a flat fake rate for both jets and electrons, the fake photon candidates are randomly selected from the jets and electrons that passed the photon acceptance requirements. One extra assumption is that the electron-to-photon fake rate is set to be order of magnitude larger than the jets-to-photon fake rate. Therefore, electrons are set to have a probability of being selected to be a misidentified photon that is ten times higher than for jets.

After the choice of fake photon candidates, we calculate weights for the individual samples based on the $E_T$ spectrum of the selected photons (prompt and fake) to match the spectrum found with the photon candidates reconstructed directly from DELPHES. This reweighting is done on the sum of $E_T$ of the two leading photons for samples with at least one prompt photon, and on the

| Process | $\sigma$ (pb) | $N_{\text{Generated}}$ | gluon Fusion | | | $ZH$ |
|---|---|---|---|---|---|---|
| | | | Asymmetric $\gamma\gamma$ | Symmetric $\gamma\gamma$ | $\gamma + E_{\text{T}}^{\text{miss}}$ | |
| Backgrounds | | | | | | |
| $\gamma$ + Jets | $1.0 \times 10^5$ | 5425448 | $1.9 \times 10^{-6}$ | $4.7 \times 10^{-7}$ | $8.9 \times 10^{-7}$ | $\approx 0$ |
| $Z$ + Jets | $0.94 \times 10^4$ | 1888446 | $5.6 \times 10^{-4}$ | $1.5 \times 10^{-4}$ | $5.0 \times 10^{-5}$ | $\approx 0$ |
| $W$ + Jets | $2.96 \times 10^4$ | 5263872 | $6.2 \times 10^{-4}$ | $1.9 \times 10^{-4}$ | $2.7 \times 10^{-5}$ | $\approx 0$ |
| $\gamma\gamma$ | $10.8 \times 10^1$ | 4268781 | $3.1 \times 10^{-5}$ | $1.0 \times 10^{-5}$ | $1.1 \times 10^{-5}$ | $\approx 0$ |
| $Z\gamma$ | $6.30 \times 10^2$ | 3406151 | $4.3 \times 10^{-4}$ | $1.4 \times 10^{-4}$ | $5.7 \times 10^{-5}$ | $\approx 0$ |
| $W\gamma$ | $1.03 \times 10^3$ | 5258034 | $1.4 \times 10^{-4}$ | $4.6 \times 10^{-5}$ | $5.4 \times 10^{-5}$ | $\approx 0$ |
| $WW$ | $1.24 \times 10^2$ | 8059829 | $2.6 \times 10^{-1}$ | $8.4 \times 10^{-2}$ | $9.8 \times 10^{-5}$ | $8.2 \times 10^{-8}$ |
| $ZZ$ | $1.8 \times 10^1$ | 1101611 | $1.4 \times 10^{-2}$ | $4.7 \times 10^{-3}$ | $6.7 \times 10^{-4}$ | $7.3 \times 10^{-6}$ |
| $WZ$ | $5.1 \times 10^1$ | 3319770 | $3.6 \times 10^{-1}$ | $1.2 \times 10^{-1}$ | $2.5 \times 10^{-4}$ | $2.9 \times 10^{-6}$ |
| Signals | | | | | | |
| Res., M = 10 GeV | $10.8 \times 10^1$ | 4268781 | $2.5 \times 10^{-4}$ | $2.2 \times 10^{-4}$ | $1.7 \times 10^{-4}$ | $5.7 \times 10^{-4}$ |
| Res., M = 40 GeV | $6.30 \times 10^2$ | 3406151 | $8.7 \times 10^{-3}$ | $5.7 \times 10^{-3}$ | $5.0 \times 10^{-3}$ | $6.9 \times 10^{-3}$ |
| Res., M = 60 GeV | $1.03 \times 10^3$ | 5258034 | $1.6 \times 10^{-2}$ | $1.1 \times 10^{-2}$ | $1.1 \times 10^{-2}$ | $9.2 \times 10^{-3}$ |
| Non-Res., M = 10 GeV | $1.24 \times 10^2$ | 8059829 | $1.5 \times 10^{-3}$ | $9.5 \times 10^{-4}$ | $1.1 \times 10^{-3}$ | $1.1 \times 10^{-3}$ |
| Non-Res., M = 40 GeV | $1.8 \times 10^1$ | 1101611 | $8.0 \times 10^{-3}$ | $5.5 \times 10^{-3}$ | $5.2 \times 10^{-3}$ | $6.3 \times 10^{-3}$ |
| Non-Res., M = 60 GeV | $5.1 \times 10^1$ | 3319770 | $1.1 \times 10^{-2}$ | $7.6 \times 10^{-3}$ | $6.9 \times 10^{-3}$ | $8.1 \times 10^{-3}$ |

Table 2: Cross sections, numbers of events generated per process, and selection efficiencies for background processes and signal points, for gluon fusion and $ZH$ production mechanisms.

$E_T$ of the leading photon for samples with no prompt photon. An independent reweighting is also done in $\eta$. Both reweightings reflect the different reconstruction efficiencies and energy resolutions of objects that are not reconstructed as photons. After applying the weights, we observe a good agreement between the kinematic distributions of interest arising from photons reconstructed by DELPHES and from our fake photon candidates.

# 3   Results

We present the expected sensitivity of this search in terms of the necessary $h \to \gamma\gamma + E_{\text{T}}^{\text{miss}}$ branching ratio to reach a $5\sigma$ sensitivity for an assumed integrated luminosity of 100 fb$^{-1}$, with the sensitivity defined as:

$$\mathcal{S} = \frac{N_{\text{Signal}}}{\sqrt{N_{\text{Background}}}}. \tag{3}$$

In Figure ??, we show the sensitivity plot for the different trigger scenarios of the gluon fusion case. This plot shows that, after the full selection, the performance of the triggers is comparable. Although it's safe to assume that a diphoton trigger with a low $M(\gamma\gamma)$ cut will be present in the future trigger menus of CMS and ATLAS, we choose to perform the analysis in the $\gamma + E_{\text{T}}^{\text{miss}}$ case. We make this choice as an effort to make the case for the existence of such a trigger strategy for the following runs of the LHC. While the diphoton triggers are designed with specific usages that are already well stablished, the $h \to \gamma\gamma + E_{\text{T}}^{\text{miss}}$ analysis could be viewed as a benchmark for the $\gamma + E_{\text{T}}^{\text{miss}}$ trigger for three reasons:

- It's a trigger that is already present at the LHC experiments, but can be retuned with a specific analysis as benchmark;

- A dedicated trigger for this analysis requiring two photons might not be as efficient at trigger legel, given the soft spectrum of the second photon;

5

- This trigger can also be used for other exotic searches, such as the extension to low energies of the dark matter searches in the monophoton channel.
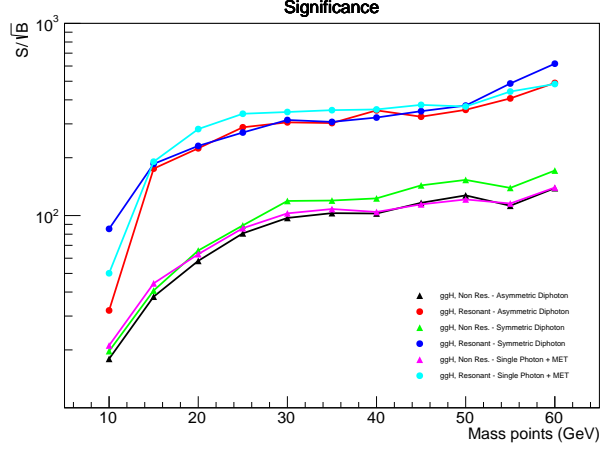


Figure 2: Significance plots for different trigger scenarios in the gluon fusion analysis.

In Figure **??**, on the left, we show the branching ratio of $h \to \gamma\gamma + E_{\mathrm{T}}^{\mathrm{miss}}$ needed for a significance of $5\sigma$, assuming the Standard Model Higgs cross section, for the gluon fusion analysis (assuming the $\gamma + E_{\mathrm{T}}^{\mathrm{miss}}$ trigger strategy and selection). On the right, we show the branching ratio $h \to \gamma\gamma + E_{\mathrm{T}}^{\mathrm{miss}}$ needed for a significance of $2\sigma$, which represents the 95% confidence level for exclusion, assuming SM $ZH$ production. We assume the channel in which the Z decays to electrons to have efficiencies and background composition that are similar to the muon case, therefore, we multiply the significance by a factor of 1.4 to obtain the full reach of the $Z \to ll$ channel.

For the $ZH$ case, we also show the analysis strategy done by CMS for Run I, requiring only one photon. The selection on table **??** remains the same, except for the subleading photon requirement and $M(\gamma\gamma)$ cut. Variables reconstructed with the diphoton information, such as $M_T(\gamma\gamma, E_{\mathrm{T}}^{\mathrm{miss}})$, are then reconstructed with the single photon information.

## 3.1 Systematic Uncertainties

While the uncertainties in the $ZH$ channel is expected to be dominated by statistics, the gluon fusion channel is very sensitive to the systematic uncertainties associated with the background predictions. We estimate the effect of these uncertainties by parametrizing the sensitivity as:

$$\mathcal{S}_{sys} = \frac{N_{\mathrm{Signal}}}{\sqrt{N_{\mathrm{Background}} + \sigma_{sys} \times N_{\mathrm{Background}}}}, \tag{4}$$

with $\sigma_{sys}$ representing a source of uncertainty that does not scale with the amount of statistics. Figure **??** shows the effect on the $5\sigma$ branching ratios due to the addition of a 10% systematic uncertainty according to Eqn **??**.

6

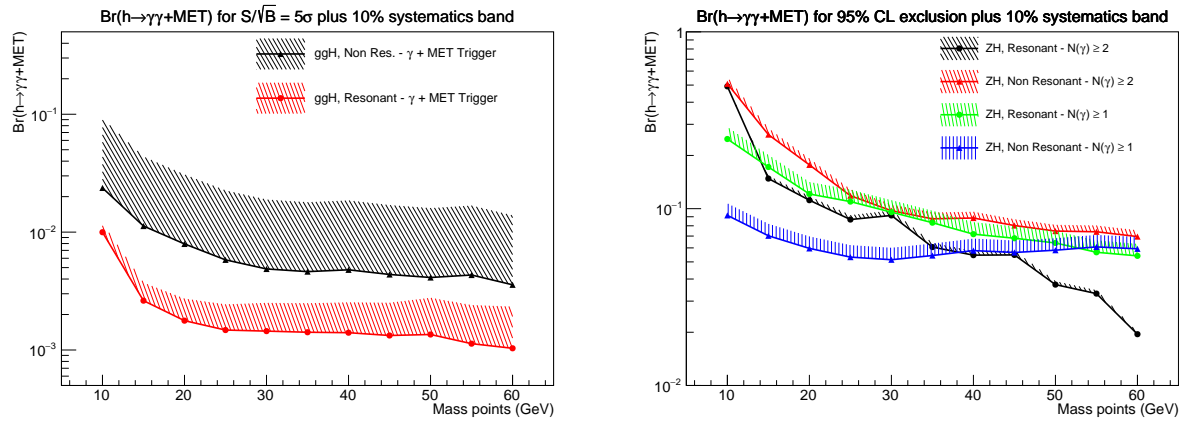Figure 3: $5\sigma$ branching ratios for the gluon fusion channel, for resonant and non-resonant final states (left). Branching ratios for 95% confidence level exclusion in the ZH case, resonant and non-resonant topologies, with single photon and diphoton selections (right).
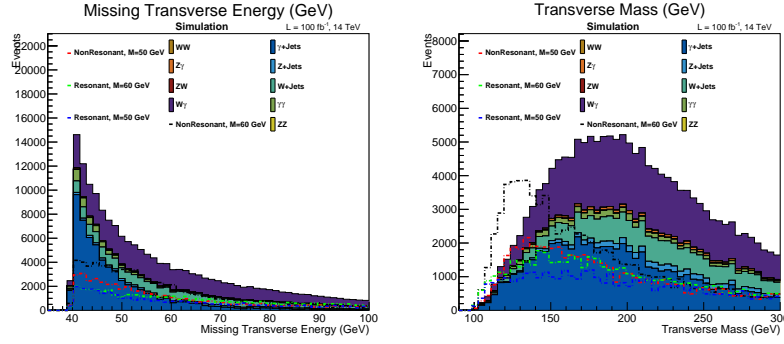
7

# 4    Additional Figures



Figure 4: (left) $E_T$ and (right) transverse mass for the gluon fusion channel.
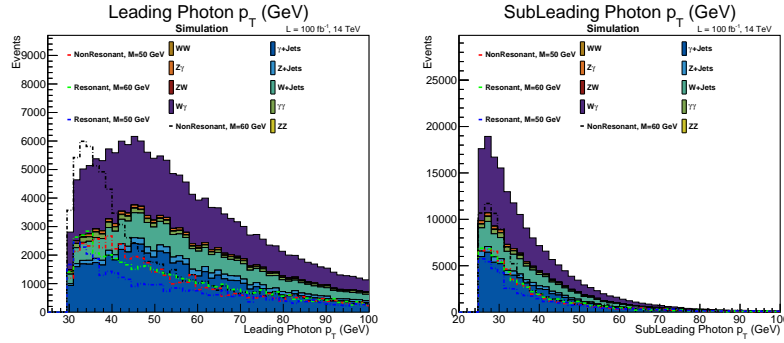


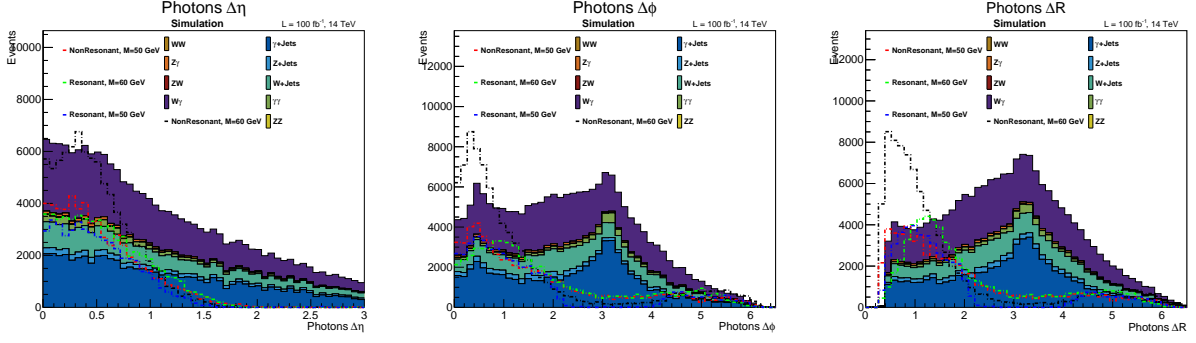Figure 5: (left) Leading photon $p_T$ and (right) subleading photon $p_T$ for the gluon fusion channel.

Figure 6: (left) $\Delta\eta$, (center) $\Delta\phi$, (right) $\Delta R$ for the gluon fusion channel.
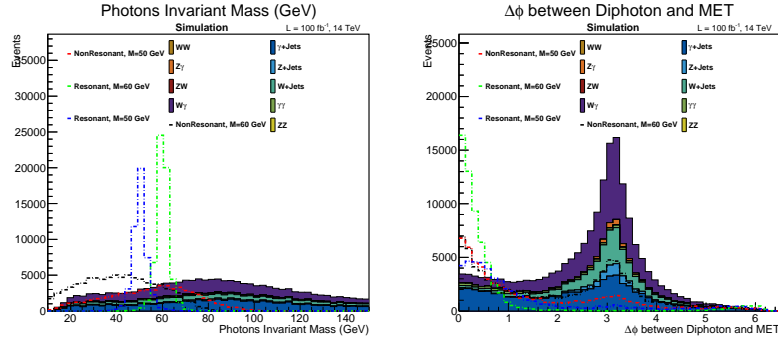


Figure 7: (left) Diphoton invariant mass and (right) $\Delta\phi$ between leading and subleading photons for the gluon fusion channel.
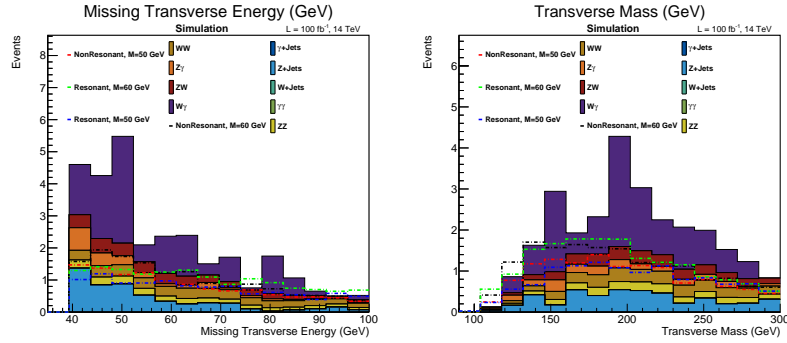


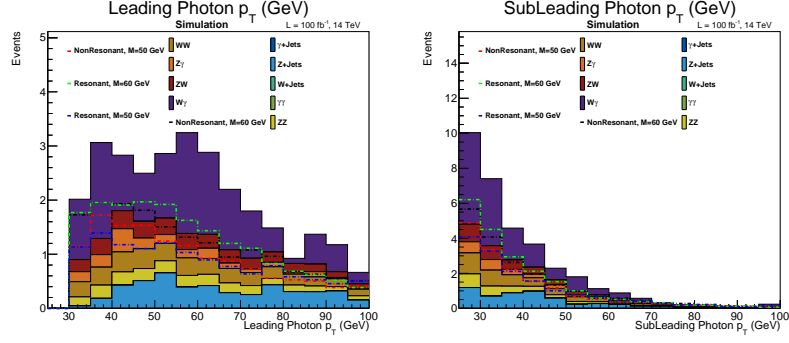Figure 8: (left) $E_{\mathrm{T}}$ and (right) transverse mass for the $ZH$ channel.

Figure 9: (left) Leading photon $p_\mathrm{T}$ and (right) subleading photon $p_\mathrm{T}$ for the $ZH$ channel.
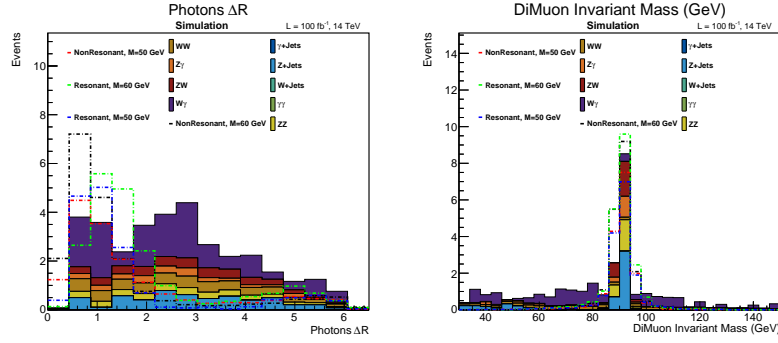


Figure 10: (left) $\Delta R$ and (right) dimuon invariant mass for the $ZH$ channel.
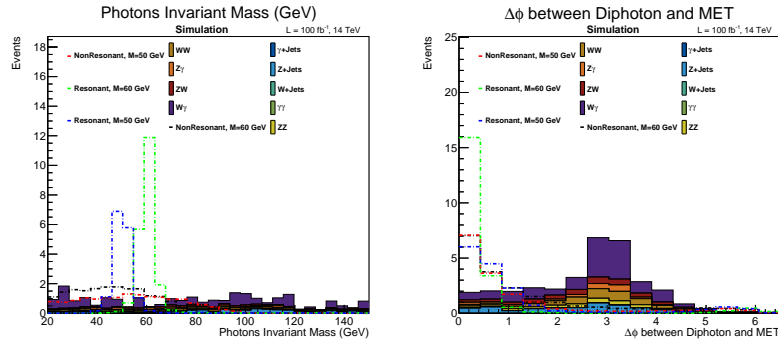


Figure 11: (left) Diphoton invariant mass and (right) $\Delta\phi$ between leading and subleading photons for the $ZH$ channel.

# 5 References

[1] D. Curtin *et al.*, Phys. Rev. D **90**, no. 7, 075004 (2014).

[2] A. Djouadi and M. Drees, Phys. Lett. B **407**, 243 (1997).

[3] J. D. Mason, D. E. Morrissey and D. Poland, Phys. Rev. D **80**, 115015 (2009) [arXiv:0909.3523 [hep-ph]].

[4] C. Petersson, A. Romagnoni and R. Torre, JHEP **1210**, 016 (2012).

[5] V. Khachatryan *et al.* [CMS Collaboration], arXiv:1507.00359 [hep-ex].

[6] The ATLAS collaboration [ATLAS Collaboration], ATLAS-CONF-2015-001.

[7] J. Alwall *et al.*, JHEP **1407**, 079 (2014).

[8] T. Sjostrand, S. Mrenna and P. Z. Skands, Comput. Phys. Commun. **178**, 852 (2008).

[9] J. de Favereau *et al.* [DELPHES 3 Collaboration], JHEP **1402**, 057 (2014).

[10] N. D. Christensen *et al.*, Eur. Phys. J. C **73** (2013) 10, 2580 doi:10.1140/epjc/s10052-013-2580-x [arXiv:1308.1668 [hep-ph]].

[11] J. Anderson *et al.*, arXiv:1309.1057 [hep-ex].

[12] J. M. Campbell and R. K. Ellis, Nucl. Phys. Proc. Suppl. **205-206**, 10 (2010) [arXiv:1007.3492 [hep-ph]].

[13] J. M. Campbell, R. K. Ellis and C. Williams, JHEP **1107** (2011) 018 doi:10.1007/JHEP07(2011)018 [arXiv:1105.0020 [hep-ph]].